

Effect of Sr Additions on the Microstructure and Strength of a Mg-Al-Ca Ternary Alloy

A. SUZUKI, N.D. SADDOCK, L. RIESTER, E. LARA-CURZIO, J.W. JONES,
and T.M. POLLOCK

The effect of Sr additions on the microstructure and strength of a Mg-5Al-3Ca alloy was investigated by replacing Ca with Sr. In the as-cast alloys, the major intermetallic compound observed at the α -Mg dendrite cell boundary region changes from the Al-rich (Mg, Al)₂Ca phase to the Mg-rich Mg₁₇Sr₂ phase with increasing Sr content. This results in an increased Al solute content in the α -Mg phase in the high-Sr containing alloys. More than 1 wt pct of Sr enhances the solid-solution strength of the α -Mg phase, resulting in the increased compression strength of the alloys.

DOI: 10.1007/s11661-006-9031-3

© The Minerals, Metals & Materials Society and ASM International 2007

I. INTRODUCTION

THE development of cost-affordable magnesium alloys is an important issue in the automotive industry as part of an effort to achieve higher fuel efficiency through vehicle weight reduction.^[1] In the last decade, there has been particular interest in creep-resistant magnesium die-cast alloys that are applicable to the powertrain components, such as engine blocks and transmission cases, which are to be exposed to the temperature range of 150 °C ~200 °C during service.^[2] The recently developed creep-resistant die-cast alloys are mainly based on the Mg-Al alloy system with Al contents of 2 to 6 wt pct and up to 4 wt pct of alloying elements including Ca, Sr, Si, or RE (RE: rare earth mishmetal, which usually consists of Ce, La, Nd, and Pr).^[3-8] The alloy design approach for attaining high-temperature creep resistance typically focuses on improving solid-solution strengthening of the α -Mg phase and increasing grain boundary strengthening by formation of intermetallic compounds that suppress the local deformation or sliding in the vicinity of grain boundaries.

The contribution of the solid-solution strength to the critical resolved shear stress $\Delta\tau$ of magnesium alloys can be generally described as follows:

$$\Delta\tau \propto \varepsilon_L^{4/3} C^{2/3}$$

where C is the solute concentration and ε_L is a parameter described as $(\eta^2 + \alpha^2\delta^2)^{1/2}$ using the size misfit parameter δ , the relative change of the shear

modulus at alloying η , and a numerical constant α ^[9,10] Among the elements listed previously, Al is the most efficient solid-solution strengthener for Mg. The atomic size misfit between Al and Mg is -11 pct,^[11] and the maximum solubility of Al in Mg is 12.6 wt pct.^[12] Other elements have larger atomic misfit than Al, but their solubility is almost zero, except for Ca, with 0.7 wt pct maximum solubility.^[13,14]

In Mg-Al-X ternary alloys where X is an element with low solubility in the α -Mg phase, the Al solute content in the primary α -Mg phase depends on the tie-line between the primary α -Mg and liquid (L) phases during solidification. At a temperature just below the liquidus temperature, the α + L tie-line lies between the primary α -Mg phase composition and the alloy composition. With decreasing temperature, the composition of the α phase shifts toward higher Al concentration according to the Mg-Al binary diagram,^[12] and the composition of the liquid phase shifts toward higher ternary element concentration. When the composition of the liquid phase reaches that of the eutectic reaction, the liquid phase starts to decompose into the α -Mg phase plus an intermetallic compound, and the alloy composition enters a three-phase tie-triangle of the L + α + intermetallic compound phases. Thus, the Al solute content in the primary α -Mg phase is determined by the partitioning of Al between the primary α -Mg and the liquid phases. In the case that the ternary element X mainly forms a Mg-rich compound as the major eutectic compound, higher Al solute content in the primary α -Mg phase can be expected than compared to the case where X is an Al-rich compound former.

Among the Mg-Al-X type alloys, the Mg-Al-Ca-based alloys are promising for the powertrain application. The alloy AXJ530, containing 5 pct Al, 3 pct Ca, and 0.15 pct Sr (wt pct), is a representative alloy with good creep resistance and castability.^[5,15,16] Recently, we have investigated the solidification paths and phase equilibria in the Mg-Al-Ca ternary system. In Mg-5 Al-3Ca, the major eutectic compound formed during

A. SUZUKI, Research Fellow, N.D. SADDOCK, Graduate Student, J.W. JONES and T.M. POLLOCK, Professors, are with the Department of Materials Science and Engineering, University of Michigan, Ann Arbor, MI 48109, USA. Contact e-mail: akanes@umich.edu L. RIESTER, Senior Technical Advisor, and E. LARA-CURZIO, Distinguished Research Staff Member, Leader, are with the Materials Science & Technology Division, Oak Ridge National Laboratory, Oak Ridge, TN 37831, USA.

Manuscript submitted June 12, 2006.

solidification is the ternary intermetallic phase (Mg, Al)₂Ca with dihexagonal C36 structure.^[17] The (Mg, Al)₂Ca phase is a relatively Al-rich compound with a composition close to Mg₂Al₄Ca₃.^[18] Therefore, the solid-solution strength of the α -Mg phase in the Mg-5Al-3Ca alloy is expected to be improved by additions of a Mg-rich compound former as a quaternary element. The improved solid-solution strength of the α -Mg phase would be beneficial to the creep resistance of these alloys in which the dislocation climb is thought to be the rate controlling process for creep deformation.^[19]

In Mg-Al based ternary systems, Sr is a potential Mg-rich compound former. Mg-Al-Sr-based alloys have been developed as creep-resistant alloys, and the die-cast AJ52x alloy (Mg-5Al-2Sr, wt pct) forms a Mg-rich phase as a major eutectic compound.^[6,7] The compound is reported to have an approximate composition of Al₃Mg₁₃Sr with an unknown crystal structure. On the other hand, the die-cast AJ51x (Mg-5Al-1Sr, wt pct) and AJ62x (Mg-6Al-2.4Sr, wt pct) alloys primarily form the Al₄Sr phase. Thus, the formation of the Mg-rich compound is expected in the relatively lower Al and higher Sr containing alloys.

In the present study, we selected Mg-5Al-3Ca (wt pct) as a base alloy composition and Sr as a quaternary element addition to explore the improvement of solid-solution strengthening of the α -Mg phase. The composition of Mg-5Al-3Ca (wt pct) is a base composition of the creep-resistant Mg-Al-Ca based alloys, such as AXJ530. The Sr was added to the base alloy composition by replacing Ca, keeping the total Ca + Sr content at 3 wt pct to examine the change in the microstructure and mechanical properties from the Mg-Al-Ca ternary system to the Mg-Al-Sr ternary system. The existing phases in as-cast materials were first investigated in the Mg-5Al-3(Ca, Sr) series alloys, and the effect of Sr addition on the solid-solution strength of the α -Mg phase was investigated by examination of the lattice parameters, compositions, and hardness measured by nanoindentation.

II. EXPERIMENTAL PROCEDURES

Table I shows the nominal and measured composition of the alloys used in this study. A series of quaternary Mg-5Al-3(Ca, Sr) (all compositions are given in weight percent unless otherwise stated) alloys were cast with the total content of Ca + Sr held constant at 3 pct. The Sr was added in increments of 0.25 to 1 pct Sr and in increments of 1 pct for the higher concentrations. These alloys are hereafter referred to by their Sr contents. The compositions of the alloys were verified by inductively coupled argon plasma emission spectrometry. These alloys were prepared using 10-kg master ingots with compositions of Mg-3.62Al-3.71Ca-0.015Mn and Mg-3.94Al-4.27Sr-0.012Mn supplied by Norsk Hydro. Compositions were adjusted with additions of 99.9 pct Mg ingot, 99.5 pct Al lump, and 99 pct Ca shot to achieve the target compositions. Each alloy with a total weight of 30 g was melted in a mild steel crucible using

Table I. Compositions of the Alloys Studied

Nominal Alloy Composition (Wt Pct)	Measured Composition (Wt Pct)		
	Al	Ca	Sr
Mg-5Al-3Ca-0Sr	5.4	3.4	< 0.01
Mg-5Al-2.75Ca-0.25Sr	5.2	3.1	0.27
Mg-5Al-2.5Ca-0.5Sr	5.1	2.7	0.52
Mg-5Al-2.25Ca-0.75Sr	4.9	2.3	0.76
Mg-5Al-2Ca-1Sr	5.3	2.3	0.99
Mg-5Al-1Ca-2Sr	5.1	1.1	2.1
Mg-5Al-0Ca-3Sr	4.9	0.01	3.0

an induction melting system with an Ar-1 pct SF₆ protective cover gas flow. The melt was stirred for a minimum of 120 s to attain homogeneity while maintaining the temperature in the range of 953 to 973 K. The material was then cooled in the crucible by turning the furnace power off, resulting in a cooling rate of about 0.6 K/s. During solidification, the temperature was recorded using a type K thermocouple and a data acquisition system to determine the liquidus and other transformation temperatures. The material was then remelted and cast into a steel mold under an Ar-1 pct SF₆ cover gas flow. Additional details on melting procedures are described in Reference 17.

Metallographic samples were cut from the ingots. The microstructure was examined by scanning electron microscopy (SEM) and transmission electron microscopy (TEM). A PHILIPS* XL30 was used for SEM

*PHILIPS is a trademark of Philips Electronic Instruments Corp., Mahwah, NJ.

studies. For TEM studies, discs of 0.12-mm thickness and 3-mm diameter were cut, mechanically polished, and then subjected to twin-jet electropolishing in a solution of methanol with 8 vol pct perchloric acid at 243 K. A PHILIPS CM12 transmission electron microscope was used in this study. Quantitative analysis of the composition of the phases was conducted using a Cameca SX-100 electron probe microanalyzer (EPMA) under an operating condition of 15 kV and 10 nA. Specimen standards used for the analysis included a Mg-4 pct Al alloy homogenized at 673 K for 623 hours, pure Al, Wollastonite (CaSiO₃), and Celestite (SrSO₄). The data within 99 to 101 total weight percent were considered as valid. The lattice parameters of the α -Mg phase were measured by powder X-ray diffraction analysis using a Rigaku X-ray diffractometer using Cu K_α radiation.

The hardness and elastic modulus of the α -Mg phase were measured with a NANOINDENTER[†] system

[†]NANOINDENTOR is a trademark of Nano Instruments, TN, USA.

equipped with a Berkovich diamond indenter. The surface of each specimen was electropolished in a

solution of methanol with 8 vol pct perchloric acid at 243 K, and the indents were made in the interior of the primary α -Mg phase. The continuous stiffness method was used in this experiment. A penetration depth of 1500 nm and a strain rate of 0.05 s^{-1} were selected. The hardness and elastic modulus were calculated using the method described in References 20 and 21. A minimum of ten measurements were obtained in each specimen. The data corresponding to indents with distorted shapes or in proximity to cell boundaries were not taken into consideration in calculating the average hardness and elastic modulus.

Specimens measuring $5 \times 5 \times 10 \text{ mm}$ in size were sectioned from the as-cast ingot for compression tests. The surface of each specimen was electropolished in a solution of methanol with 8 vol pct perchloric acid at 243 K to remove surface residual stress. Compression tests were performed using a compression fixture in a 5582 screw-driven Instron with a digital data acquisition system. The displacements between the platens were measured by linear variable differential transducers. The tests were conducted at room temperature and 448 K. For tests at 448 K, a clamshell-type resistance furnace was used. During the test, the temperature variation was maintained within $\pm 2 \text{ K}$. A strain rate of 10^{-4} s^{-1} was used in this study.

III. RESULTS AND DISCUSSION

A. Microstructure and Existing Phases of the Mg-5Al-3(Ca, Sr) Alloys

Figure 1 shows the backscattered electron (BSE) images of the as-cast Mg-5Al-3Ca (0Sr) and Mg-5Al-3Sr (3Sr) ternary alloys. Both alloys exhibit similar microstructures consisting of the α -Mg phase and intermetallic compounds. The α -Mg phase exhibits an irregular globular-shaped morphology, which corresponds to cells of the α -Mg dendrites. The average dendrite cell size is about $30 \mu\text{m}$. The 0Sr alloy (Figure 1(a)) shows two types of eutectic structures surrounding the α -Mg phase. According to our previous study,^[17] the interdendritic feature has a coarse lamellar morphology and consists of α -Mg and $(\text{Mg}, \text{Al})_2\text{Ca}$ (C36) phases. The minor one with fine lamellar morphology mainly consists of α -Mg and Mg_2Ca (C14) phases. In this Sr-free alloy, the formation of the primary α -Mg phase is followed by the $L \rightarrow \alpha + \text{C36}$ eutectic reaction, and the solidification is terminated with the ternary eutectic reaction $L \rightarrow \alpha + \text{C14} + \text{C36}$. This invariant reaction mainly forms the α -Mg and C14 phases, and the volume fraction of the C36 phase in the ternary eutectic structure is low.^[17,18] The 3Sr alloy also shows two types of intermetallic compounds (Figure 1(b)). The major compound has a blocky semicontinuous morphology with medium contrast, and the minor compound has a lamellar morphology with bright contrast. Figure 2(a) shows the TEM bright-field image (BFI) of the major compound. A series of selected area diffraction patterns (SADPs) was collected from the compound

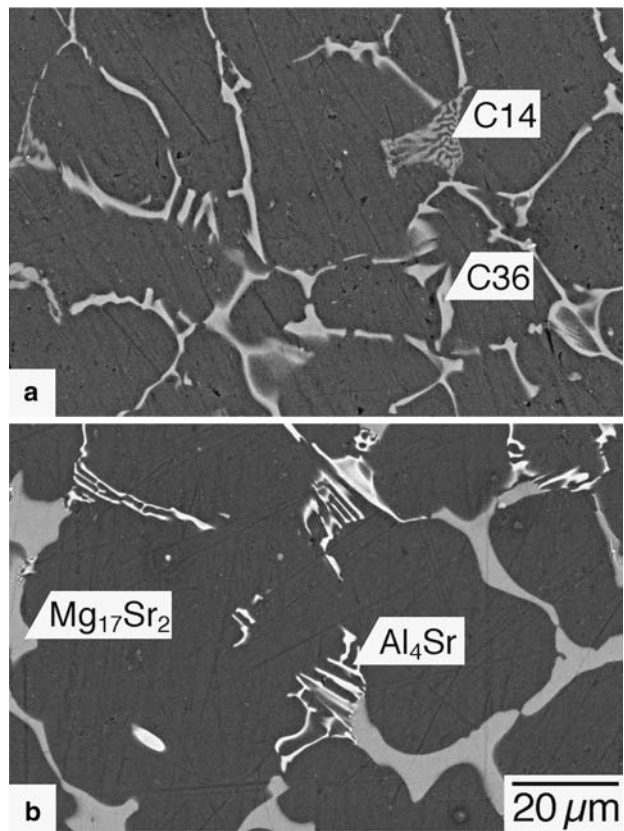


Fig. 1—BSE images of as-cast (a) Mg-5Al-3Ca and (b) Mg-5Al-3Sr ternary alloys.

by rotating the sample to identify the crystal structure. The SADP shown in Figure 2(c) was taken after 30-deg rotation from the SADP of Figure 2(b) with a fixed reciprocal lattice vector \mathbf{g}_1 . By comparing the observed SADPs with the calculated patterns, the crystal structure of the major compound was identified as hexagonal hP38 structure, and the SADPs correspond to $B = 1120$ (Figure 2(b)) and $B = 10\bar{1}0$ (Figure 2(c)). Thus, the major compound is the $\text{Mg}_{17}\text{Sr}_2$ phase. Similarly, the minor compound (Figure 2(d)) was identified as the Al_4Sr phase with tetragonal D_{13} structure. The SADPs shown in Figures 2(e) and (c) correspond to $B = 110$ and $B = 100$, respectively, which are tilted 45 deg from each other with the same vector \mathbf{g}_2 . The morphological features of these compounds are similar to those observed in the die-cast AJ52 and AJ52x alloys.^[6,7] In these die-cast alloys, the major compound was reported to be an unknown ternary phase with a tentative composition of $\text{Al}_3\text{Mg}_{13}\text{Sr}$. Formation of several ternary compounds was also reported in Reference 22 in the Mg-Al-Sr ternary system. However, the two compounds observed in this study are binary compounds with solid solubility. This result agrees with the report by Cao *et al.*^[23] that showed the absence of ternary intermetallic compounds in the Mg-rich corner of the ternary system. Thus, it is reasonable to consider that the major compound observed in the 3Sr alloy is the $\text{Mg}_{17}\text{Sr}_2$ phase with solid solubility of Al. According to the reported liquidus projection,^[23] the $\text{Mg}_{17}\text{Sr}_2$ and

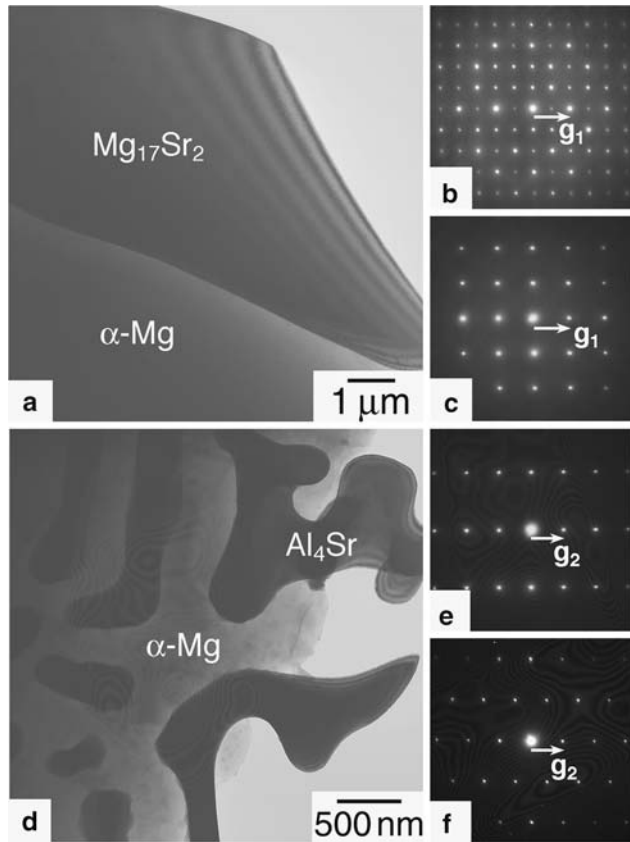


Fig. 2—TEM BFIs and SADPs taken from the intermetallic compounds in the as-cast 3Sr alloy: (a) BFI showing $Mg_{17}Sr_2$ phase, (b) $B = 11\bar{2}0$ (hP38), (c) $B = 10\bar{1}0$ (hP38), (d) BFI showing Al_4Sr phase, (e) $B = 110$ (D1₃), and (f) $B = 100$ (D1₃).

Al_4Sr phases in the 3Sr alloy are formed by the eutectic reaction $L \rightarrow \alpha + Mg_{17}Sr_2$ and the subsequent transitional invariant reaction $L + Mg_{17}Sr_2 \rightarrow \alpha + Al_4Sr$.

Figure 3 shows the BSE images of the quaternary alloys containing 0.25 pct Sr (Figure 3(a)) and 1 pct Sr (Figure 3(b)). Similar to the ternary 0Sr and 3Sr alloys, these quaternary alloys show microstructures consisting of the primary α -Mg phase with average dendrite cell size of about $30 \mu m$ and intermetallic compounds surrounding the α -Mg phase. In the 0.25Sr alloy, the major compound remains as the C36 phase. However, instead of the minor intermetallic C14 phase observed in the 0Sr alloy, Sr-rich regions containing multiple compounds were observed, as indicated in Figure 3(a). With increasing Sr content, the volume fraction of the Sr-rich region increases, while the volume fraction of the C36 phase decreases, as observed in the 1Sr alloy (Figure 3(b)). Figure 4(a) shows the TEM BFI of the Sr-rich region for the 0.5Sr alloy. The SADPs taken from the spherical-shaped phase (Figure 4(b)) and the irregular-shaped phase with dark contrast (Figure 4(c)) are identical to the patterns obtained with $B = 1120$ of the hP38 and C36 structures, respectively. Thus, the Sr-rich region is a mixture of the $Mg_{17}Sr_2$ (hP38), $(Mg, Al)_2Ca$ (C36), and α -Mg phases. From these results, the quaternary alloys consist of the α -Mg, C36, and $Mg_{17}Sr_2$ phases, and the addition of as little as 0.25

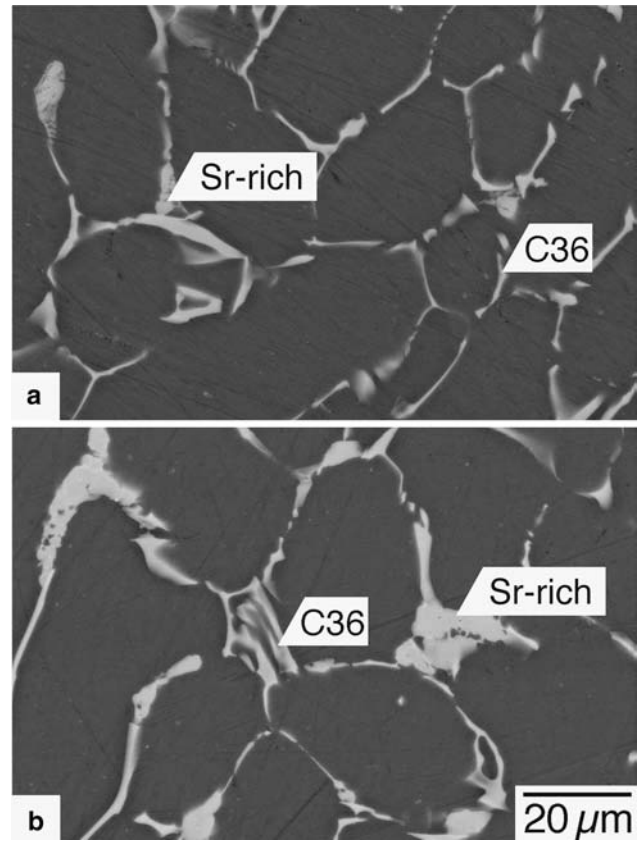


Fig. 3—BSE images of as-cast quaternary alloys: (a) 0.25Sr and (b) 1Sr.

pct Sr to the Mg-5Al-3Ca causes the formation of the $Mg_{17}Sr_2$ phase, indicating that Ca and Sr tend to separately form intermetallic compounds in this quaternary system.

Figure 5 shows the liquidus and eutectic transformation start temperatures detected by thermal analysis during solidification of the Mg-5Al-3(Ca, Sr) alloys. The temperatures are plotted against the Sr contents of the

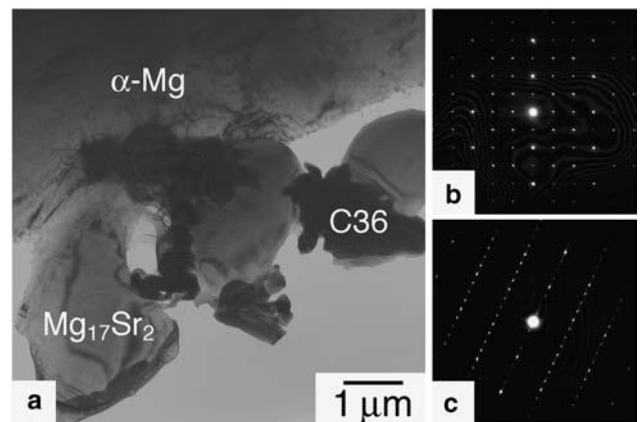


Fig. 4—TEM BFI and SADPs taken from the intermetallic compounds in the Sr-rich region at dendrite cell boundary of the as-cast 0.5Sr alloy: (a) BFI showing α -Mg, $Mg_{17}Sr_2$, and C36 phases; (b) $B = 11\bar{2}0$ (hP38); and (c) $B = 11\bar{2}0$ (C36).

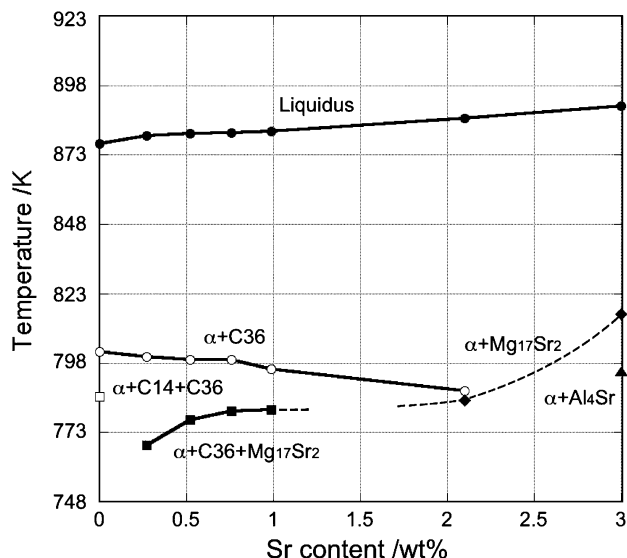


Fig. 5—Liquidus and eutectic transformation temperatures detected by thermal analysis during solidification.

alloys. The liquidus temperature slightly increases with Sr content from 877 to 890 K. On the other hand, the $L \rightarrow \alpha + C36$ eutectic temperature decreases from 802 K in the 0Sr alloy to 788 K in the 2Sr alloy. The formation temperature of the Sr-rich region consisting of the α -Mg, C36, and $Mg_{17}Sr_2$ phases is lower than 773 K in the 0.25Sr alloy, and it increases with Sr addition. This result indicates that Sr tends to be concentrated into the liquid phase during solidification and that the solidification of the quaternary alloys is terminated with the formation of the $Mg_{17}Sr_2$ phase.

From these results, the major eutectic compound changes from the Al-rich C36 phase to the Mg-rich $Mg_{17}Sr_2$ phase with additions of Sr, and this is expected to increase the Al solute content in the primary α -Mg phase.

B. Effect of Sr Additions on the α -Mg Phase in the Mg-5Al-3(Ca, Sr) Alloys

Figure 6 shows the lattice parameters of the α -Mg phase measured by X-ray diffraction. Both a and c values slightly increase with Sr addition up to 0.5 pct and then decrease abruptly in the range of 0.5 to 1 pct, with more gradual decrease with further Sr additions beyond 1 pct. From these lattice parameter measurements, the investigated quaternary alloys can be divided into two groups: low-Sr (0 to 0.5 pct) and high-Sr (1 to 3 pct) alloys. While the lattice parameters must be closely related to the composition of the α -Mg phase, the composition cannot be precisely determined in as-cast alloys because of the presence of the composition gradient in the α -Mg phase. However, assuming that the Ca and Sr solute content is negligibly low, the measured lattice parameters were compared with the reported values of the α -Mg solid-solution phase in the binary Mg-Al alloys.^[24] The estimated Al solute

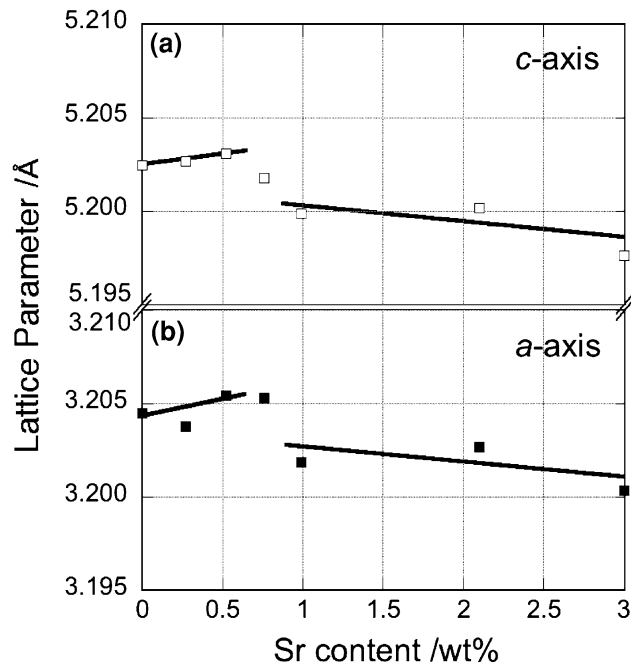


Fig. 6—Lattice parameters of the α -Mg phase plotted against Sr content of the alloys.

contents in the low-Sr ($a \sim 3.205 \text{ \AA}$, $c \sim 5.203 \text{ \AA}$) and high-Sr ($a \sim 3.202 \text{ \AA}$, $c \sim 5.199 \text{ \AA}$) alloys were approximately 1.7 and 2.2 pct, respectively.

The composition of the α -Mg phase was quantitatively examined by EPMA in the low-Sr and high-Sr alloys. In each sample, at least six α -Mg dendrite cells were randomly selected, and composition measurements were conducted across each dendrite cell in 4- μm intervals. Figure 7 shows the measured compositions in the 0.25Sr alloy plotted against the normalized distance from the center of α -Mg dendrite cells where 0 and 1 correspond to the center and edge of each dendrite cell, respectively. At the dendrite cell center, the Mg content is about 98 pct, and it decreases to about 97 pct toward cell boundaries, while the Al content increases from about 2 to 2.5 pct. The Ca content is almost constant at about 0.2 pct, regardless of the analyzed position. The Sr content is nearly zero at all locations in each dendrite cell. To compare the compositions of the dendrite cell center in the different Sr content alloys, the data taken from the region where the normalized distance from the center is between 0 and 0.25 were sorted, and five data points with the lowest Al content were averaged in each alloy. This is because the position of the dendrite core that is expected to have the lowest alloying content cannot be unambiguously determined from the two-dimensional microstructure revealed by standard metallographic samples. Similarly, among the data taken from the region where the normalized distance from the center is between 0.6 and 0.8, five data points with the highest Al content were averaged to compare the composition of the region close to dendrite cell boundaries. The data in the region between 0.8 and 1 were not used, because those were

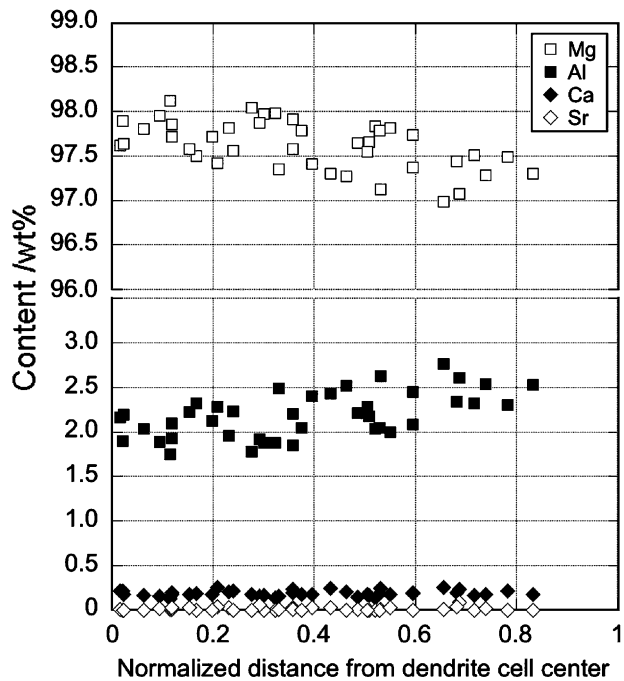


Fig. 7—The composition of the α -Mg phase of the 0.25Sr alloy plotted against the normalized distance from the dendrite cell center. The dendrite cell center is at 0.

presumed to be affected by the existence of the intermetallic compounds.

Figure 8 shows the Al and Ca contents of the α -Mg phase plotted against the Sr content of the alloys. The Al content in the dendrite cell center region clearly shows the composition difference between the low-Sr and high-Sr alloys: about 1.8 pct in the 0 to 0.5 pct Sr alloys and about 2.2 pct in the 1 to 3 pct Sr alloys. The Al content

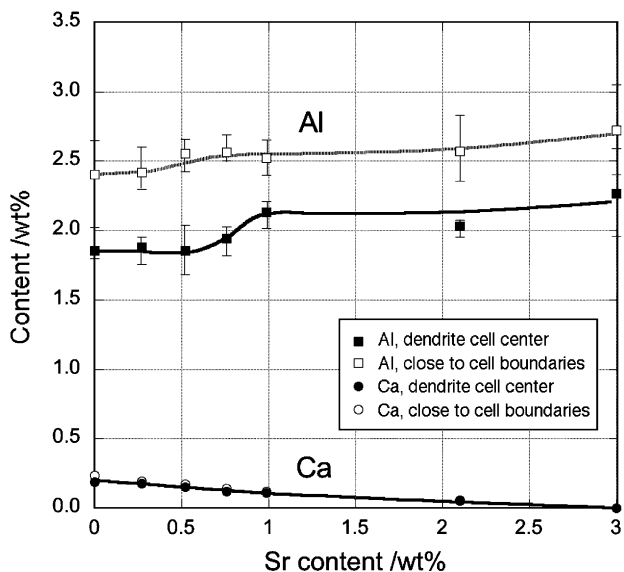


Fig. 8—Al and Ca contents of the α -Mg phase in the regions close to dendrite cell center and cell boundaries, plotted against the Sr content of the alloys.

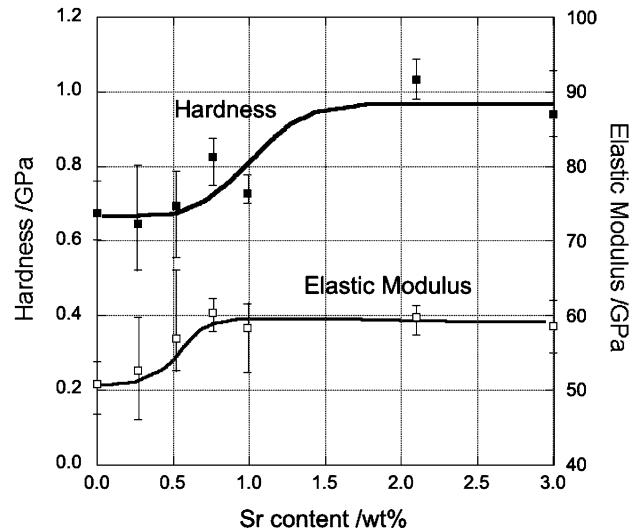


Fig. 9—Hardness and elastic modulus of the α -Mg phase measured by nanoindentation.

in the region close to dendrite cell boundaries monotonically increases from 2.4 to 2.7 pct with Sr addition. The Ca content is less than 0.2 pct and linearly decreases with Sr addition. The Sr solute content was less than 0.1 pct in all of the samples.

The difference in the Al solute content between low-Sr and high-Sr alloys and the monotonic decrease in Ca content suggest that a difference in the solid-solution strength of the α -Mg phase between these alloys is likely. To evaluate the strength of the α -Mg phase, the hardness of the α -Mg phase was measured by nanoindentation. By using the constant indentation depth at 1500 nm, indents of about 10 μm in size were made in the dendrite cell interiors. The maximum load during the indentation was about 50 mN. Because the average dendrite cell size is about 30 μm , these indents are small enough to eliminate the effect of dendrite cell boundary intermetallic compounds. Figure 9 shows the hardness and the elastic modulus of the α -Mg phase measured by nanoindentation. The hardness is about 0.7 GPa in the low-Sr alloys up to 0.5 pct Sr, and it increases to about 1 GPa with the increase in Sr content. The elastic modulus also exhibits an increase from 50 to 60 MPa in the low-Sr content regime.

These results demonstrate that the addition of Sr to the Mg-5Al-3Ca alloy increases the solid-solution strength of the α -Mg phase by increasing the Al solute content, and that at least 1 pct Sr additions are necessary to obtain the increased strength. The hardening contribution of the Ca is apparently much lower, compared to Al.

C. Partitioning of Al during Solidification

The difference in the Al solute content in the α -Mg phase can be qualitatively explained by considering the solidification paths of the alloys. Figure 10 shows the superimposed liquidus projections of the Mg-Al-Ca^[17] and Mg-Al-Sr^[23] ternary systems. Using the thermal

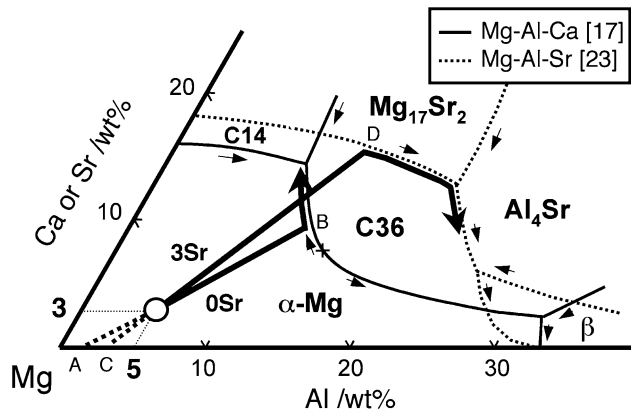


Fig. 10—Solidification paths of the 0Sr and 3Sr alloys drawn on the liquidus projections of the Mg-Al-Ca^[17] and Mg-Al-Sr^[23] ternary systems.

analysis data obtained during solidification of 0Sr and 3Sr alloys, the solidification paths that the liquid phase follows during solidification were estimated and depicted with thick lines in Figure 10. In the 0Sr alloy, the formation and growth of the primary α -Mg phase is followed by the $L \rightarrow \alpha + C36$ eutectic reaction, and the solidification is terminated with the ternary eutectic reaction $L \rightarrow \alpha + C14 + C36$. The tie-line between α -Mg and the liquid phase corresponds to the line AB in Figure 10, and the Al content at point A approximately corresponds to the maximum Al solute content in the α -Mg phase, because the Ca solute content is close to zero. Similarly, in the 3Sr alloy, the eutectic compounds are formed by the eutectic reactions $L \rightarrow \alpha + Mg_{17}Sr_2$ and $L \rightarrow \alpha + Al_4Sr$ via a transitional peritectic reaction $L + Mg_{17}Sr_2 \rightarrow \alpha + Al_4Sr$, and the point C corresponds to the maximum Al solute content in the α -Mg phase. Comparison of the $\alpha + L$ tie-lines in the 0Sr and 3Sr alloys, AB and CD, shows the difference in the partitioning of Al between the phases; the partitioning ratio of Al, $k_{\alpha/L}^{Al}$, in the 0Sr alloy is lower than that in the 3Sr alloy. The difference in the Al partitioning behavior results in the formation of the Al-rich C36 compound in the 0Sr alloy and the Mg-rich $Mg_{17}Sr_2$ compound in the 3Sr alloy as major eutectic compounds.

Based on this idea, other elements that can form Mg-rich compounds have a potential for improving the solid-solution strength of the α -Mg phase. Other potential elements include Si, Sn, and Ga, which form the Mg_2Si ,^[3,25] Mg_2Sn ,^[26] and Mg_5Ga_2 ^[27] phases, respectively, based on the reported liquidus projections.

In the composition analysis described here, the composition of the α -Mg phase showed a jump in Al solute content between 0.5 and 1 pct Sr content (Figure 8). However, it is difficult to predict the minimum Sr addition that is necessary to appreciably increase the Al solute content based on the available ternary diagrams. The development of more reliable thermodynamic databases will be useful to predict the partitioning behavior of elements in multicomponent alloys.

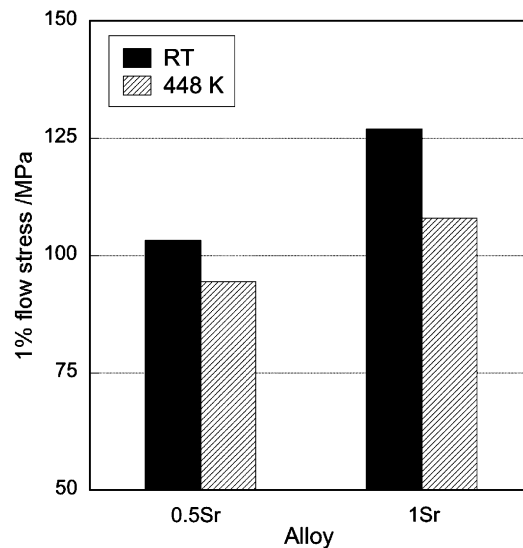


Fig. 11—One percent flow stress of the 0.5Sr and 1Sr alloys measured in compression at room temperature and 448 K.

D. Contribution of the Solid-Solution Strengthening of the α -Mg Phase to the Strength of Alloys

According to the study by Caceres and Rovera^[28] on the solid-solution strength of Mg-Al alloys, the 0.2 pct proof strength σ_p can be expressed as $\sigma_p = \sigma_0 + kd^{-1/2} + mB_nC^n$. The last term, mB_nC^n , corresponds to the solid-solution strength, where B_n is the solid-solution hardening rate on the basal plane (21.2 or 39.5 MPa(at.)^{-2/3}), m is the Taylor factor (5.6 or 5) when $n = 1/2$ or $2/3$, respectively, and C is the Al atom concentration. Using this relation for the increment of solid-solution strengthening, we would predict an increase in flow stress between 16 MPa ($n = 1/2$) and 39 MPa ($n = 2/3$) for a change in the Al content from 1.8 to 2.2 wt pct, which are the approximate Al contents in the dendrite cell center of the low-Sr and high-Sr alloys, respectively (Figure 8). Figure 11 shows the 1 pct flow stress of the 0.5Sr and 1Sr alloys measured in compression at room temperature and 448 K. The flow stress of the 0.5Sr alloy is about 105 MPa at room temperature and about 95 MPa at 448 K. The 1Sr alloy shows higher values than the 0.5Sr alloy at both temperatures, about 125 and 110 MPa, respectively. The difference in the flow stress between the 0.5Sr (low-Sr) and 1Sr (high-Sr) alloys at room temperature is about 20 MPa, which is in the range of the predicted amount based on the change in the Al solute content. Therefore, the change in the compression strength from the low-Sr to high-Sr alloys can be attributed to the solid-solution strengthening by Al.

However, in addition to the change in the Al solute content, the intermetallic compounds at dendrite cell boundaries also change with Sr content in the examined alloys, as described in Section III-A. While the dendrite cell boundaries may serve as sources of dislocations for deformation, it is not immediately clear how changes in the observed intermetallic compounds could influence the overall deformation process. Further investigation

using high-resolution strain mapping techniques^[29] would give further insight to the contribution of the intermetallic compounds and solid-solution strength of the α -Mg phase to the overall strength of the alloys.

Another important problem to consider is that the high-temperature creep resistance of magnesium die-cast alloys does not always follow the same trend with the tensile strength.^[30] This would be partly related to the microstructural instability at elevated temperatures, because phases existing in as-cast materials are not always the same as the equilibrium phases at the creep test temperatures. Therefore, understanding of the as-solidified microstructure as well as phase equilibria and transformation kinetics at lower temperatures is essential for the development of high creep-resistant alloys.

IV. CONCLUSIONS

1. In Mg-5Al-3(Ca, Sr) alloys, additions of Sr greater than 1 pct improve the solid-solution strength of the α -Mg phase by increasing the Al solute content, resulting in an increase in the compression strength.
2. The increased Al solute content by additions of more than 1 pct Sr is caused by the change in the partitioning of Al between the primary α -Mg and liquid phases. The higher partitioning of Al to the α -Mg phase in the high-Sr containing alloys (>1 pct) results in the formation of the Mg-rich Mg₁₇Sr₂ phase as a major eutectic compound, while the major eutectic compound in the low-Sr containing alloys (<0.5 pct) is the Al-rich compound, (Mg, Al)₂Ca phase.
3. The obtained results in this study suggest that the additions of elements that form Mg-rich compounds as major eutectic phases offer a potential means to modify the solid-solution strength of the α -Mg phase and thus improve the strength and creep resistance.

ACKNOWLEDGMENTS

This research was supported by NSF FRG Grant No. DMR-0309468 and the Assistant Secretary for Energy Efficiency and Renewable Energy, Office of Freedom Car and Vehicle Technologies, as part of the High Temperature Materials Laboratory User Program, Oak Ridge National Laboratory, managed by UT-Battelle, LLC, for the United States Department of Energy under Contact No. DE-AC05-000R22725. The authors are thankful to C.J. Torbet, C. Henderson (University of

Michigan), Dr. B.R. Powell, N. Irish (General Motors), and Dr. P. Bakke (Norsk Hydro) for their assistance.

REFERENCES

1. S. Das: *JOM*, 2003, vol. 55(11), pp. 22–26.
2. B.R. Powell, L.J. Ouiment, J.E. Allison, J.A. Hines, R.S. Beals, L. Kopka, and P.P. Ried: in *Magnesium Technology 2004*, A.A. Luo, ed., TMS, Warrendale, PA, 2004, pp. 3–10.
3. A.A. Luo: *Int. Mater. Rev.*, 2004, vol. 49, pp. 13–30.
4. M.O. Pekguleryuz and A.A. Kaya: in *Magnesium Alloys and Their Applications*, K.U. Kainer, ed., Wiley-VCH Verlag GmbH, Germany, 2003, pp. 74–93.
5. A.A. Luo, M.P. Balogh, and B.R. Powell: *Metall. Mater. Trans. A*, 2002, vol. 33A, pp. 567–74.
6. M.O. Pekguleryuz and E. Baril: *Mater. Trans.*, 2001, vol. 42, pp. 1258–1267.
7. E. Baril, P. Labelle, and M.O. Pekguleryuz: *JOM*, 2003, vol. 55(11), pp. 34–39.
8. P. Bakke and H. Westengen: in *Magnesium Technology 2005*, N.R. Neelameggham, H.I. Kaplan and B.R. Powell, eds., TMS, Warrendale, PA, 2005, pp. 291–96.
9. P. Haasen: in *Physical Metallurgy*, R.W. Cahn and P. Haasen, eds., Vol. 3, Elsevier Science, Amsterdam, Netherlands, 1996, 4th ed., pp. 2033.
10. P. Lukac: *Phys. Status Solidi (a)*, 1992, vol. 131, pp. 377–90.
11. R. Ferro and A. Saccone: in *Physical Metallurgy*, R.W. Cahn and P. Haasen, eds., Vol. 1, Elsevier Science, Amsterdam, Netherlands, 1996, 4th ed., pp. 329.
12. H. Okamoto: *J. Phase Equilibria*, 2003, vol. 24, p. 580.
13. H. Okamoto: *Phase Diagrams for Binary Alloys*, ASM INTERNATIONAL, Metals Park, OH, 2000.
14. H. Okamoto: *J. Phase Equilibria*, 1998, vol. 19, p. 490.
15. B.R. Powell, A.A. Luo, V. Rezhets, J.J. Bommarito, and B.L. Tiwari: *SAE Trans.: J. Mater. Manufacturing*, 2001, vol. 110, pp. 406–13.
16. A.A. Luo, M.P. Balogh, and B.R. Powell: *SAE Trans.: J. Mater. Manufacturing*, 2001, vol. 110, pp. 414–22.
17. A. Suzuki, N.D. Saddock, J.W. Jones, and T.M. Pollock: *Acta Mater.*, 2005, vol. 53, pp. 2823–34.
18. A. Suzuki, N.D. Saddock, J.W. Jones, and T.M. Pollock: *Metall. Mater. Trans. A*, 2006, vol. 37A, pp. 975–83.
19. Y. Terada, N. Ishimatsu, R. Sota, T. Sato: *Metall. Mater. Trans. A*, 2007, vol. 38A, in press.
20. M. Radovic, E. Lara-Curzio, and L. Riestler: *Mater. Sci. Eng.*, 2004, vol. A368, pp. 56–70.
21. W.C. Oliver and G.M. Pharr: *J. Mater. Res.*, 1992, vol. 7, pp. 1564–83.
22. M.A. Parvez, M. Medraj, E. Essadiqi, A. Muntasar, and G. Denes: *J. Alloys Compounds*, 2005, vol. 402, pp. 170–85.
23. H. Cao, J. Zhu, C. Zhang, K. Wu, N.D. Saddock, J.W. Jones, T.M. Pollock, R. Schmid-Fetzer, and Y.A. Chang: *Z. Metallkd.*, 2006, vol. 97, pp. 422–28.
24. J.L. Murray: *Bull. Alloy Phase Diagrams*, 1982, vol. 3, pp. 60–74.
25. E. Schurmann and A. Fischer: *Giessereiforschung*, 1977, vol. 29, pp. 161–65.
26. E.M. Semenova: *Dokl. Akad. Nauk SSSR*, 1969, vol. 188, pp. 1308–10.
27. K.A. Bol'shakov, P.I. Fedorov, E.I. Smarina, and I.N. Smirnova: *Russ. J. Inorg. Chem.*, 1964, vol. 9, pp. 1020–27.
28. C.H. Caceres and D.M. Rovera: *J. Light Met.*, 2001, vol. 1, pp. 151–56.
29. N.E. Biery, M. DeGraef, and T.M. Pollock: *Metall. Mater. Trans. A*, 2003, vol. 34A, pp. 2301–13.
30. I.P. Moreno, T.K. Nandy, J.W. Jones, J.E. Allison, and T.M. Pollock: *Scripta Mater.*, 2003, vol. 48, pp. 1029–34.